The influence of porosity on nanoparticle formation in hierarchical aluminophosphates

Matthew E. Potter[1]*, Lauren N. Riley[1], Alice E. Oakley[1], Panashe M. Mhembere[1], June Callison[2,3] and Robert Raja[1]*

[1]Department of Chemistry, University of Southampton, Highfield Campus, Highfield, Southampton, SO17 1BJ, UK.
[2]UK Catalysis Hub, Research Complex at Harwell, Rutherford Appleton Labs, Harwell Campus, OX11 0FA, UK.
[3]Department of Chemistry, University College London, 20 Gordon Street, London, WC1H 0AJ, UK.

Email: *Matthew E. Potter; M.E.Potter@soton.ac.uk, Robert Raja; R.Raja@soton.ac.uk

ORCid iDs: Matthew E. Potter (0000-0001-9849-3306), Alice E. Oakley (0000-0002-5489-9424), Panashe Mhembere (0000-0002-1219-8486), June Callison (0000-0003-4506-1862), Robert Raja (0000-0002-4161-7053).

Abstract

The ability to tailor metal active sites is increasingly important, due to the superior advantages in nanoparticle utilisation in a diverse range of fields. One of the key factors that determines the properties of immobilised nanoparticles is metal-support interactions, thus the nature of the support is crucial for optimising nanoparticle design for a range of catalytic applications. In this work we explore the deposition of gold onto a silicoaluminophosphate, using a variety of known nanoparticle deposition techniques. By comparing the gold particles deposited on a traditional microporous aluminophosphate, with an analogous hierarchical species, containing both micropores and mesopores, we explore the influence of this dual porosity on nanoparticle deposition. We show that the presence of mesopores has limited influence on the nanoparticles properties, but allows the system to maintain porosity after nanoparticle deposition. This will aid diffusion of reagents through the system, allowing continued access the active sites in hierarchical systems, which offers significant potential in catalytic oxidation/reduction reactions.

Keywords

Aluminophosphate; Catalysis; Hierarchical catalysts; Nanoparticles; Porosity

Findings

The controlled synthetic design of metallic nanoparticles has generated significant interest in recent decades, due to their implementation in a range of fields including medicine [1], optics [2] and catalysis [3]. Given the wide range of controllable properties, such as size, shape and charge, nanoparticle design is non-trivial, as specific procedures are constantly being developed to promote targeted features and behaviours [4]. Commonly in catalysis nanoparticles are immobilised onto a solid support, preventing aggregation, leading to increased catalyst lifetime and performance [5]. Yet, immobilisation further complicates nanoparticle design by introducing surface-nanoparticle interactions, which have been shown to have a significant influence on their catalytic efficacy [6]. Commonly, the supports used are porous, which allows the nanoparticle to be deposited, and yet sufficiently isolated from other particles, to hinder aggregation. Of the wide range of supports utilised in the literature, micro- and meso-porous species are the most common [7-10]. Microporous materials can achieve high levels of control in catalytic reactions, resulting in targeted product selectivity and hence are, in principle, excellent hosts for metal nanoparticles [11]. Similarly, zeotype materials such as zeolites and aluminophosphates (AlPOs) also possess a wide range of secondary functionalities that could synergise with the nanoparticles in a catalytic reaction [12]. However due to the limited pore windows and channels of these systems, even sub-nanometre particles can block the framework and hinder activity, thereby preventing reagents from accessing the internal active sites. In contrast, mesoporous species (pores > 2 nm) maintain a large portion of their porosity when hosting metal nanoparticles, though lack the more subtle ability to control the space around the active site [13]. In our previous work we have shown that inclusion of a micellular agent; DMOD (Dimethyloctadecyl[3-(trimethoxysilyl)propyl] Ammonium Chloride) in an AlPO synthesis, alongside a microporous template, allows silanol-lined mesopores, to form simultaneously, alongside with the microporous network, yielding a hierarchically porous (HP) system [14]. In this work we utilise both a HP silicoaluminophosphate (SAPO) system and a traditional microporous SAPO-5 species, to demonstrate the advantages of hierarchical systems for nanoparticle deposition. We selected SAPO-5 as our basic framework, as the AlPO-5 synthesis is robust, and forms one of the largest AlPO frameworks (pore size 7.3 Å), which will aid nanoparticle deposition and maintain porosity. Specifically we compare three known nanoparticle preparation methods; incipient wetness (IW), wet-impregnation (WI) and ammonia evaporation (AE) on the typical microporous (MP-SAPO-5) and corresponding hierarchically porous system (HP-SAPO-5) [15,16].

MP-SAPO-5 was synthesised according to our previous work [17], giving the expected phase-pure, crystalline, microporous AlPO-5 framework (Figures 1A, S1-S3 and Table S2). Modifying the synthesis procedure by adding a small quantity of DMOD (Table S1) into the hydrothermal gel (HP-SAPO-5) preserved the phase-purity, as only AlPO-5 features are present (Figure S1). Nitrogen physisorption measurements shows that while the type I isotherm of MP-SAPO-5 strongly indicates microporosity, HP-SAPO-5 has a type IV isotherm, indicating the hierarchical nature of the sample (Figure S2), though with a disordered mesoporous region. This is typical of hierarchical materials prepared in this manner [12,14] as they contain a broad range of mesopore sizes. Subsequent pore-distribution plots show no textural features for MP-SAPO-5 in the 20 – 350 Å region, but HP-SAPO-5 shows a discerning hysteresis, indicating mesopores, which are 60 Å in size (Figure S3). This is also highlighted as both systems possess similar micropore pore volumes, though HP-SAPO-5 has a much larger mesopore pore volume. The particles of HP-SAPO-5 were notably less crystalline than MP-SAPO-5 (Figure 1). The HP-SAPO-5 showed crystalline features were present, with smaller crystalline particles aggregating, forming part of a platelet morphology. The features of the HP-SAPO-5 are attributed to the DMOD used in the synthesis. The DMOD is believed to modify the crystallisation rates, which allows mesopores to form. In doing it also increases the disorder in the system, leading to this agglomeration and different crystalline phases. Overall we concluded that the bare HP-SAPO-5 and MP-SAPO-5 systems were successfully synthesised. They were then used as supports for gold deposition, to explore the influence the microporous and hierarchical systems had on the nanoparticles characteristics.

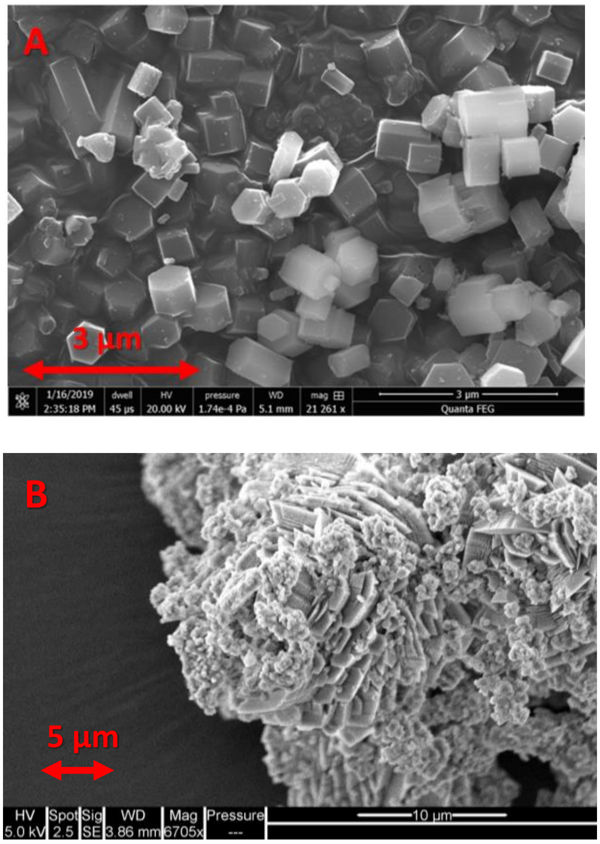

Figure 1: SEM images of microporous MP-SAPO-5 (A) and hierarchical HP-SAPO-5 (B).

All three deposition methods (IW, WI and AE) were carried out on both HP-SAPO-5 and MP-SAPO-5, with an intended theoretical loading of 1 wt% of Au. Metal analysis on the deposited MP-SAPO-5 (Table S3) shows the gold loadings vary significantly depending on the immobilisation strategy used, with IW being the most effective (0.66 wt% Au) and WI being the least (0.10 wt% Au). Likely the minimal amount of solvent used in the IW method increases support-metal interactions leading to more rapid deposition. The minimal solvent will also be readily adsorbed into the internal pores of the material by capillary action, encouraging the metal to deposit on the micropores and mesopores, and not just on the external surface. In contrast the excess solvent in WI will promote deposition primarily on the external surface. AE has reasonable deposition efficiency (0.49 wt% Au), likely the evaporation stage of this process also encourages limited capillary action, similar to IW. Excellent agreement is seen between analogous MP-SAPO-5 and HP-SAPO-5 systems (Table S3), suggesting that the inclusion of silanol-lined mesopores neither encourages, nor hinders, nanoparticle deposition.

Following nanoparticle deposition, all samples maintained a phase-pure AlPO-5 framework, with the powder XRD patterns showing no significant variation in crystallinity or signal width (Figures 2, S4 & S5). Nanoparticle deposition was found to greatly reduce the porosity of both the hierarchical and microporous supports. For MP-SAPO-5 the surface area decreases from 254 m^2/g to just 72 m^2/g, on depositing 0.10 wt% of Au through WI (Figure S6 and Table S4). This is accompanied by a significant decrease in pore volume (Table S4). Given the framework integrity is maintained (Figures S4 & S5), the decrease in porosity suggests the 1D channels are blocked, restricting access to the internal micropores. As pore-mouths are known to produce high energy defect sites [18], they are more likely to encourage nanoparticle deposition, thus blocking the AlPO-5 channels. IW and AE methods decrease the surface area to a greater extent, due to increased Au deposition. The surface area follows a similar trend for HP-SAPO-5, with bare support > WI > AE > IW, again in agreement with the Au loadings (Figure 2B, Tables S3 & S4). Notably a higher proportion of porosity is maintained in the hierarchical systems, where equivalent loadings of gold give surface areas above 110 m^2/g. The surface areas for the Au-doped MP systems were difficult to estimate due to a loss of data at the very lowest pressures, however the measurements here provide a reasonable estimate (Table S4). Further qualitative comparison of the isotherms for the Au-doped MP and HP at low pressure confirms the significantly lower surface area in the MP systems. The total pore volume follows a similar trend, with higher Au loadings prompting lower pore volumes, however for the hierarchical system a higher proportion of the pore volume still remains on deposition (Table S4). Thus the introduction of mesopores into the hierarchical system (Figure S7) helps the systems maintain higher pore volumes and surface areas after nanoparticle inclusion. In principle this should translate into the hierarchical systems being improved catalysts with better diffusion.

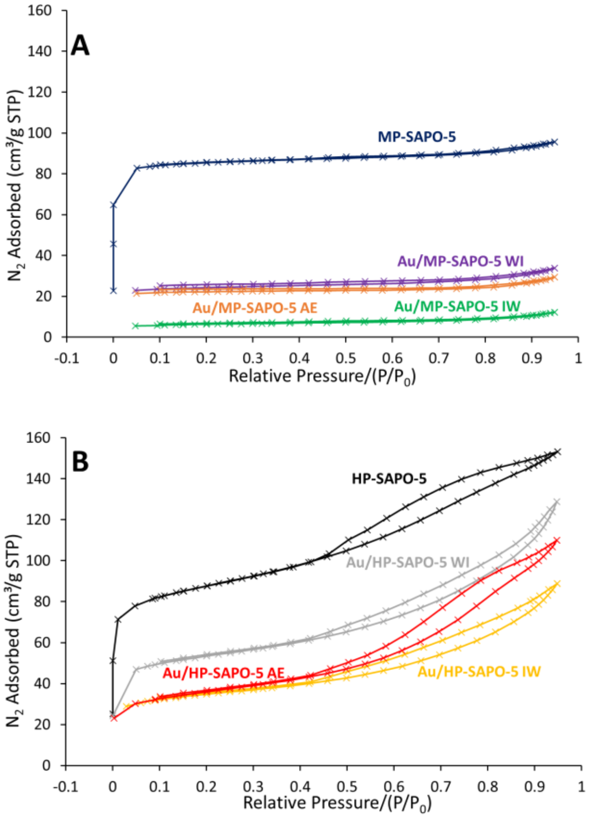

Figure 2: Nitrogen physisorption isotherms of gold-deposited microporous (A) and hierarchical (B) SAPO-5 systems showing porosity is maintained in hierarchical HP-SAPO-5, but not microporous MP-SAPO-5.

To probe the influence of the support on the metals deposited, a range of characterisation techniques were used to explore the nature of the Au species. UV/Vis measurements show signals attributed to localised surface plasmon resonance for both Au/MP-SAPO-5 (Figure S8) and Au/HP-SAPO-5 (Figure S9) systems suggesting nanoparticles have indeed formed *via* the IW and AE procedures

[19]. However, no signals are seen for WI samples due to the low (0.10 wt%) Au loadings. The peak positions are in good agreement for the Au/MP-SAPO-5 species between the two techniques (IW 514 nm, AE 517 nm), though the hierarchical system shows a greater disparity (IW 511 nm, AE 529 nm). This is likely due to the wider range of possible deposition sites and environments, though overall the systems are in good agreement. X-ray adsorption spectroscopy (XAS) was used to probe the gold species, but only subtle variations between the systems was observed (Figures 3 & S10-S15). There was good agreement with the Au foil, suggesting the gold has been successfully reduced to metallic gold particles. The Au/MP-SAPO-5 systems show a lower energy XANES edge, suggesting a higher average oxidation state ($Au^{\delta+}$, Figure S11) than the Au foil (Au^0) [20]. In all cases the data was satisfactorily fit with a single Au-Au path, at a bond distance of 2.85-2.86 Å (Figure 3 and Table 1). The Au coordination number for all Au/SAPO-5 systems was found to be lower than the theoretical value of 12 for bulk Au foil, suggesting the formation of non-bulk Au systems. In both systems the coordination number was found to vary as AE < IW < WI, indicating AE produces smaller sized nanoparticles [21], despite WI having significantly lower Au loading. This again emphasises the influence of synthesis protocols on active site design.

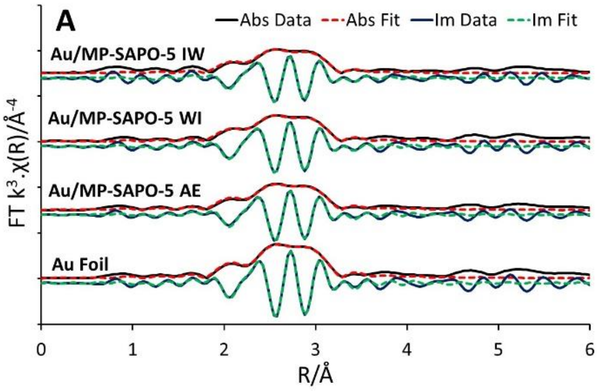

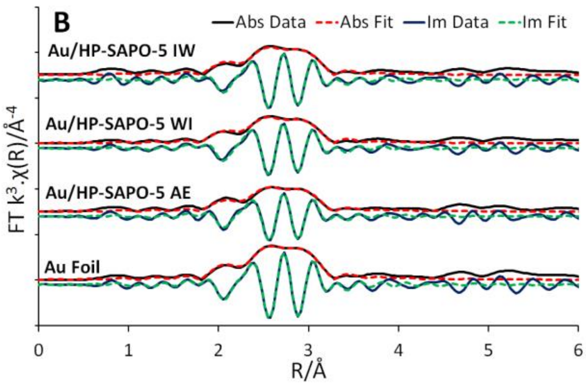

Figure 3: The magnitude and imaginary component of the k^3 weighted Fourier transform for the EXAFS data of the Au-deposited microporous MP-SAPO-5 (A) and hierarchical HP-SAPO-5 (B) compared to the Au foil. Associated scattering paths, with a single Au-Au feature are included.

Table 1: EXAFS fitting paths of Au-doped SAPO systems and Au foil.

Sample	Abs Sc	N	R/Å	$2\sigma^2$/Å^2	R_{factor}
Au/MP-SAPO-5 IW	Au-Au	10.0 (5)	2.849 (5)	0.0088 (5)	0.019
Au/MP-SAPO-5 WI	Au-Au	11.2 (3)	2.850 (3)	0.0089 (4)	0.006
Au/MP-SAPO-5 AE	Au-Au	10.1 (3)	2.852 (3)	0.0083 (3)	0.007
Au/HP-SAPO-5 IW	Au-Au	10.7 (4)	2.855 (5)	0.0082 (4)	0.015
Au/HP-SAPO-5 WI	Au-Au	10.8 (4)	2.851 (4)	0.0087 (5)	0.012
Au/HP-SAPO-5 AE	Au-Au	9.3 (4)	2.854 (5)	0.0082 (3)	0.020
Au Foil	Au-Au	12 (fixed)	2.857 (2)	0.0077 (1)	0.004

Fitting parameters: S_0^2 value of 0.826, determined by Au foil standard; fit range $3.0 < k < 12.3$ and $1.5 < R < 3.5$, number of independent points = 11.7, Abs Sc = absorbing atom – scattering atom.

XPS data (Figure 4) was in good agreement with the XAS data, as Au/HP-SAPO-5 IW and Au/HP-SAPO-5 AE systems were exclusively fit with Au^0 features (Figure 4B). However the corresponding microporous systems required additional Au^1 features to be accurately fit, in agreement with the $Au^{\delta+}$ species observed from by

XANES (Figure 4A). As XPS has a limited penetration depth, it will accentuate surface species, which are more likely to contain Au^1 species, over the bulk [22]. In both cases the weak signal from the low loading of the WI systems makes fitting infeasible. These measurements confirm that the different porosity of the two systems has only a subtle influence on the nanoparticle environment and coordination. A potential cause of this being the lack of porosity in the Au/MP-SAPO-5 species, hindering the complete reduction of the Au species, during the activation (calcination/reduction) process.

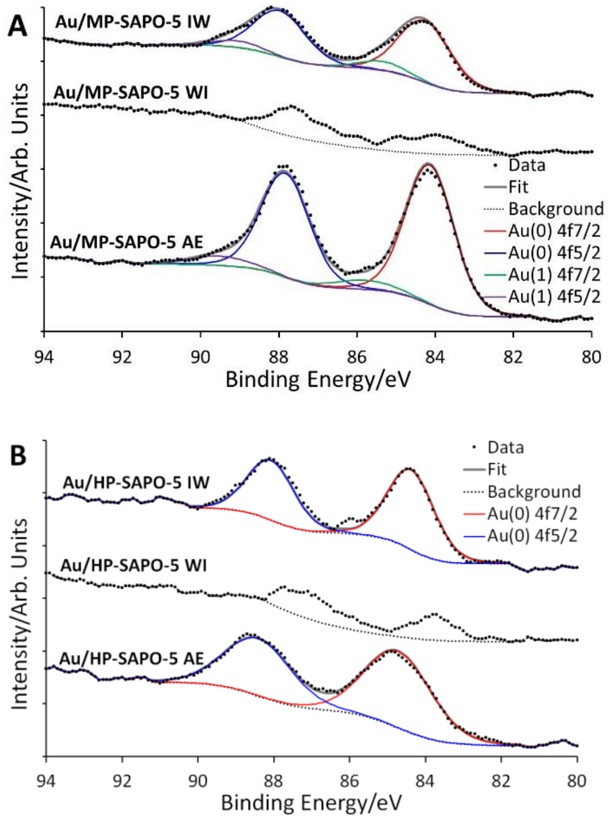

Figure 4: Stacked XPS data for Au-doped microporous MP-SAPO-5 (A) and hierarchical HP-SAPO-5 (B) showing the oxidation states present in the samples.

We have thus shown that pore blockage can be minimised by immobilising metal nanoparticles onto hierarchical systems, allowing tailored zeotype catalysts to act as hosts through the inclusion of mesopores, with their inherent porosity aiding nanoparticle reduction. Such materials have potential in catalytic oxidations/reductions, with Au/HP-SAPO-5 IW yielding a TON of 35 (Table S5) for the catalytic oxidation of toluene (preliminary findings). These materials offer significant potential as catalysts in their own right for C-H activation, but also as nanoparticle hosts. The dual porosity opens up the possibility of selectively isolating distinct active sites in specific-sized pores, towards intelligently designed bifunctional and tandem catalysts.

Supporting Information (if any)

File Name: Supplementary Information

File Format: Text and Figures

Title: Supplementary Information

Acknowledgements (optional)

Panashe Mhembere acknowledges AdvanSix and Honeywell LLC for financial support. Dr. Matthew Cooper and the Geochemistry group at the National Oceanography Centre, University of Southampton are thanked for their help performing and analysing the ICP-MS data. The UK Catalysis Hub is kindly thanked for resources and support provided via our membership of the UK Catalysis Hub Consortium and funded by EPSRC grant: EP/R026815/1. The authors wish to acknowledge the Diamond Light Source and the UK Catalysis Hub for provision of beamtime (proposal number SP19850-2). Dr. Mark Isaacs and HarwellXPS are thanked for their assistance collecting the XPS data for this work.

References

1. Lohse, S. E.; Murphy, C. J. *J. Am. Chem. Soc.* **2012**, *134*, 15607-15620.

2. Lal, S.; Link, S.; Halas, N. J. *Nat. Photon.* **2007**, *1*, 641-648.

3. Prati, L.; Villa, A. *Acc. Chem. Res.* **2014**, *47*, 855-863.

4. Rogers, S. M.; Catlow, C. R. A.; Chan-Thaw, C. E.; Gianolio, D.; Gibson, E. K.; Gould, A. L.; Jian, N.; Logsdail, A. J.; Palmer, R. E.; Prati, L.; Dimitratos, N.; Villa, A.; Wells, P. P. *ACS Catal.* **2015**, *5*, 4377-4384.

5. Dimitratos, N.; Lopez-Sancez, J. A.; Hutchings, G. J. *Chem. Sci.* **2012**, *3*, 20-44.

6. Prieto, G.; Zečević J.; Friedrich, H.; de Jong, K. P.; de Jongh, P. E. *Nat. Mater.* **2013**, *12*, 34-39.

7. Zhu, Q.-L.; Li, J.; Xu, Q. *J. Am. Chem. Soc.* **2013**, *135*, 10210-10213.

8. Farrusseng, D.; Tuel, A. *New. J. Chem.* **2016**, *40*, 3933-3949.

9. Cruz, P.; Pérez, Y.; del Hierro, I.; Fajardo, M. *Micropor. Mesopor. Mater.* **2016**, *220*, 136-147.

10. Chen, Y.; Zhu Q.-L.; Tsumori, N.; Xu, Q. *J. Am. Chem. Soc.* **2014**, *137*, 106-109.

11. O’Malley, A. J.; Parker, S. F.; Chutia, A.; Farrow, M. R.; Silverwood, I. P.; Garcia-Sakai, V.; Catlow, C. R. A. *Chem. Commun.* **2016**, *52*, 2897-2900.

12. Raja, R.; Potter, M. E.; Newland, S. H. *Chem. Commun.* **2014**, *50*, 5940-5957.

13. Potter, M. E.; Purkis, J. M.; Perdjon, M.; Wells, P. P.; Raja, R. *Mol. Syst. Des. Eng.* **2016**, *1*, 335-344.

14. Newland, S. H.; Sinkler, W.; Mezza, T.; Bare, S. R.; Carravetta, M.; Haies, I. M.; Levy, A.; Keenan, S.; Raja, R. *ACS Catal*. **2015**, *5*, 6587-6593.

15. White, R. J.; Luque, R.; Budarin, V. L.; Clark, J. H.; Macquarrie, D. J. *Chem. Soc. Rev.* **2009**, *38*, 481-494.

16. Zhu, S.; Gao, X.; Zhu, Y.; Fan, W.; Wang, J.; Li, Y. *Catal. Sci. Technol.* **2015**, *5*, 1169-1180.

17. Potter, M. E.; Kezina, J.; Bounds, R.; Carravetta, M.; Mezza, T. M.; Raja, R. *Catal. Sci. Technol.* **2018**, *8*, 5155-5164.

18. Wei, F.-F.; Cui, Z.-M.; Meng, X.-J.; Cao, C.-Y.; Xiao, F.-S.; Song, W.-G. *ACS Catal.* **2014**, *4*, 529-534.

19. Mori, K.; Verma, P.; Hayashi, R.; Fuku, K.; Yamashita, H. *Chem. Eur. J.* **2015**, *21*, 11885-11893.

20. Malta, G.; Kondrat, S. A.; Freakley, S. J.; Davies, C. J.; Lu, L.; Dawson, S.; Thetford, A.; Gibson, E. K.; Morgan, D. J.; Jones, W.; Wells, P. P.; Johnston, P.; Catlow, C. R. A.; Kiely, C. J.; Hutchings, G. J. *Science* **2017**, *355*, 1399-1403.

21. Beale, A. M.; Weckhuysen, B. M. *Phys. Chem. Chem. Phys.* **2010**, *12*, 5562-5574.

22. Casaletto, M. P.; Longo, A.; Martorana, A.; Prestianni, A.; Venezia, A. M. *Surf. Interfaces Anal.* **2006**, *38*, 215-218.